THE JOURNAL OF PHYSICAL CHEMISTRY B

Article

Cite This: J. Phys. Chem. B 2019, 123, 4705−4717

pubs.acs.org/JPCB

Polarized Two-Photon Absorption and Heterogeneous Fluorescence Dynamics in NAD(P)H

Published as part of The Journal of Physical Chemistry virtual special issue "Hai-Lung Dai Festschrift".

Thomas S. Blacker,[†,‡,§] Nick Nicolaou,[†] Michael R. Duchen,[§] and Angus J. Bain*[,†,‡]

[†]Department of Physics & Astronomy, University College London, Gower Street, London WC1E 6BT, United Kingdom

[‡]Centre for Mathematics and Physics in the Life Sciences and Experimental Biology (CoMPLEX), University College London, Gower Street, London WC1E 6BT, United Kingdom

[§]Research Department of Cell & Developmental Biology, University College London, Gower Street, London WC1E 6BT, United Kingdom

ABSTRACT: Two-photon absorption (2PA) finds widespread application in biological systems, which frequently exhibit heterogeneous fluorescence decay dynamics corresponding to multiple species or environments. By combining polarized 2PA with time-resolved fluorescence intensity and anisotropy decay measurements, we show how the two-photon transition tensors for the components of a heterogeneous population can be separately determined, allowing structural differences between the two fluorescent states of the redox cofactor NAD(P)H to be identified. The results support the view that the two states correspond to alternate configurations of the nicotinamide ring, rather than folded and extended conformations of the entire molecule.

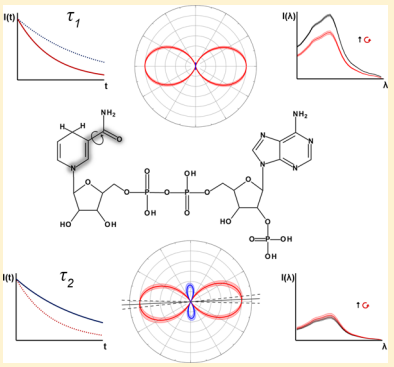

INTRODUCTION

NAD and NADP are the principle biological cofactors involved in cellular redox metabolism.[1] The two molecules differ only by the presence of a phosphate group at the redox-inactive adenine end of NADP which is absent in NAD, as shown in Figure 1. This allows enzyme binding sites to be specific to either cofactor, enabling them to regulate contrasting biochemical pathways. The hydride-carrying nicotinamide ring is identical in the two molecules, and it is responsible for the spectrally identical intrinsic fluorescence of their reduced forms, NADH and NADPH.[2] As alterations in the redox balance of the NAD and NADP pools are linked to a range of pathological conditions, NAD(P)H autofluorescence is often employed to investigate the role of metabolism in disease.[3] Fluorescence lifetime imaging microscopy (FLIM) is frequently used for this purpose; inside cells, the rate of decay of NAD(P)H fluorescence is dependent upon the enzymes to which the molecules are bound, allowing changes in the metabolic pathways activated in the diseased state to be detected in a label-free manner.[3−8] Maximizing the information content of these measurements requires an increased understanding of how the photophysical quantities reported reflect the biochemical status of the target molecules.

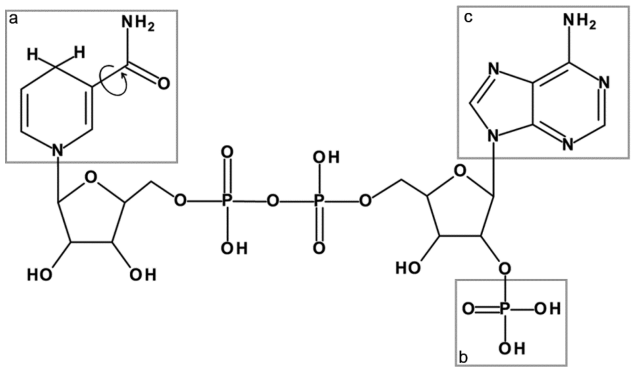

Figure 1. Fluorescence in NADH and NADPH is localized to the nicotinamide moiety (a), where the amide group can adopt a *cis* (shown) or *trans* form by rotating 180° around the bond linking it to the pyridine ring. NADPH differs in structure from NADH by the presence of a phosphate group (b) at the adenine (c) end of the molecule.

Even outside the highly crowded and nonuniform environment of the cell,[9] pure aqueous solutions of NADH or NADPH exhibit fluorescence decay dynamics indicative of an intrinsically heterogeneous population.[10−12] Two species are present in solutions of either molecule, a majority component (∼90%) with a lifetime of approximately 0.4 ns and a minority component (∼10%) of 0.8 ns.[10] However, the molecular origin of these species remains elusive. NAD(P)H is known to exist

Received: March 29, 2019
Revised: April 25, 2019
Published: April 25, 2019

DOI: 10.1021/acs.jpcb.9b01236
J. Phys. Chem. B 2019, 123, 4705−4717

in two distinct configurations in solution, either folded with stacked adenine and nicotinamide rings or open and extended,[13] and parallels have perhaps naively been drawn between these two configurations and the two-component fluorescence decay of the molecule. For example, it has been suggested that the short lifetime state results from the folded configuration inducing dynamic quenching of the excited nicotinamide by the adenine moiety.[14,15] In contrast, the apparent nonexistence of the longer lifetime state in NAD(P)H analogues where the adenine moiety is absent led to suggestions that the nicotinamide and adenine rings form an exciplex with an enhanced quantum yield when stacked.[11,16] Recent ultrafast transient absorption studies appear to rule this out.[17] Additionally, inconsistencies between the decay amplitudes of the two components and the fraction of folded species measured by energy transfer,[13] alongside demonstrations of heterogeneous decay kinetics in nicotinamide mononucleotide,[12,18,19] suggest that the two fluorescence decay times arise from photophysical processes independent of the adenine moiety.

In previous work, we demonstrated that the high rate of nonradiative excited state decay in NAD(P)H is due to small scale motion of the nicotinamide ring.[10] Power law models implied that the specific molecular motion associated with the conformational relaxation was identical in the two species, while an activated barrier crossing analysis suggested that the contrasting lifetimes of the two species arise from differences in the shape of the intramolecular potential energy surface experienced by the molecule while undergoing the motion. In the present study, we gain further insight into the photophysical origins of the two excited state populations in NAD(P)H through a novel approach to determine the individual two-photon absorption (2PA) properties of a multiple component system.

Polarization Dependence of Two-Photon Absorption. A fundamental property of single-photon absorption (1PA) in an isotropic medium is that the transition probability is independent of the polarization of the incident light.[20] However, for 2PA, the transition does not involve a simple dipolar rearrangement of electronic charge density but depends on a sum of products of all the allowed single-photon electric dipole transition moments between the ground, virtual, and final states. In essence, the first photon can be thought of as selecting a nonstationary virtual state that can be caused to undergo transitions to the final state by a second photon with only certain polarizations.[21,22] The polarization dependence of 2PA is most commonly expressed through the polarization ratio Ω, defined as the ratio of the 2PA cross sections for circularly and linearly polarized excitation[23]

$$\Omega = \frac{\sigma_{2P}^{circ}}{\sigma_{2P}^{lin}} \tag{1}$$

The orientation-dependent transition probability for the absorption of two identical photons with polarization vectors $\hat{e}$ can be expressed as[24,25]

$$A_{2PA} = |\hat{e}\cdot\underline{\mathbf{S}}\cdot\hat{e}|^2 \tag{2}$$

where $\underline{\mathbf{S}}$ is the second rank tensor describing the angular properties of the two-photon transition. Transforming from the laboratory to molecular frame of reference and performing the necessary orientational averaging is most conveniently achieved using a spherical tensor formalism.[22,24−27] With this approach and assuming a planar transition, valid for NAD(P)H,[2] Ω can be written as

$$\Omega = \frac{(S_{XX}+S_{YY})^2 + 3(S_{XX}-S_{YY})^2 + 12(S_{XY})^2}{4(S_{XX}+S_{YY})^2 + 2(S_{XX}-S_{YY})^2 + 8(S_{XY})^2} \tag{3}$$

Normalizing with respect to S_{XX} yields[22,24−27]

$$\Omega = \frac{(1+S)^2 + 3(1-S)^2 + 12D^2}{4(1+S)^2 + 2(1-S)^2 + 8D^2} \tag{4}$$

where $S = S_{YY}/S_{XX}$ and $D = S_{XY}/S_{XX}$. Values of Ω range from $^1/_4$ to $^3/_2$ depending on the symmetry of the participating electronic and vibrational states[23,26−38] and local solvation effects.[39] The fluorescence anisotropies immediately after excitation by linearly and circularly polarized 2PA, $R_{lin}(0)$ and $R_{circ}(0)$ respectively, are also determined by the components of $\underline{\mathbf{S}}$ according to[25]

$$R_{lin}(0) = \frac{1}{7}\left[1 + \frac{9[(1-S^2)(\cos^2\theta_M - \sin^2\theta_M) + 4(1+S)D\sin\theta_M\cos\theta_M]}{2(1+S)^2 + (1-S)^2 + 4D^2}\right] \tag{5}$$

$$R_{circ}(0) = \frac{1}{7}\left[\frac{(1+S)^2 - 3[(1-S)^2 + 4D^2] - 6[(\cos^2\theta_M - \sin^2\theta_M)(1-S^2) + 4D(1+S)\sin\theta_M\cos\theta_M]}{(1+S)^2 + 3(1-S)^2 + 12D^2}\right] \tag{6}$$

where θ_M is the angle made by the emission transition dipole with respect to the x-axis of the molecular frame. Adopting a coordinate system in which this is defined by the direction of the 1PA transition dipole moment, θ_M can be determined from the initial anisotropy following 1PA[40]

$$R_{1P}(0) = \frac{2}{5}\left[\frac{3\cos^2\theta_M - 1}{2}\right] \tag{7}$$

Thus, given experimental measurements of $R_{lin}(0)$, $R_{circ}(0)$, $R_{1P}(0)$, and Ω, the corresponding two-photon tensor components S and D can be calculated by solving eqs 4−7. This approach has previously been applied to perylene[26,27,36] and enhanced green fluorescent protein (EGFP).[25] As Ω is independent of emission dipole moment orientation, it has also been measured by time averaged (steady state) fluorescence intensities following linearly and circularly polarized 2PA. However, as will be seen, this approach is no longer possible in systems with strongly heterogeneous fluorescence dynamics such as NAD(P)H, and it is necessary to combine both time-resolved and steady state fluorescence measurements to

DOI: 10.1021/acs.jpcb.9b01236
J. Phys. Chem. B 2019, 123, 4705−4717

determine the individual Ω values and corresponding transition tensor structures of each species.

Polarized Two-Photon Excited Fluorescence in Heterogeneous Systems. The simplest heterogeneous system corresponds to a mixed population containing two species i = 1, 2 with relative (ground state) abundances γ_i (with $\gamma_1 + \gamma_2 = 1$), radiative rates k_i^{rad} and fluorescence lifetimes τ_i. The fluorescence decays following linearly and circularly polarized two-photon excitation are given by

$$I_{circ}(t) = A_{circ}[\gamma_1\sigma_1^{circ}k_1^{rad}\exp(-t/\tau_1) + \gamma_2\sigma_2^{circ}k_2^{rad}\exp(-t/\tau_2)] \quad (8)$$

$$I_{lin}(t) = A_{lin}[\gamma_1\sigma_1^{lin}k_1^{rad}\exp(-t/\tau_1) + \gamma_2\sigma_2^{lin}k_2^{rad}\exp(-t/\tau_2)] \quad (9)$$

where σ_i^{circ} and σ_i^{lin} are the cross sections for circularly and linearly polarized 2PA. The parameters A_{circ} and A_{lin} account for differences in the amount of fluorescence collected in each decay measurement arising, for example, from variations in laser power and collection times. In steady state measurements, A_{circ} and A_{lin} can be made equal by measuring time-averaged fluorescence count rates under constant illumination intensity. Under these conditions, using eqs 8 and 9 to equate the ratio of absorption strengths to the ratio of fluorescence intensities[29] gives

$$\bar{\Omega} = \frac{\langle I_{circ}(t)\rangle}{\langle I_{lin}(t)\rangle} = \frac{\int_0^\infty I_{circ}(t)\,dt}{\int_0^\infty I_{lin}(t)\,dt} = \frac{\gamma_1\sigma_1^{circ}\varphi_1 + \gamma_2\sigma_2^{circ}\varphi_2}{\gamma_1\sigma_1^{lin}\varphi_1 + \gamma_2\sigma_2^{lin}\varphi_2} \quad (10)$$

where the bar signifies that the single $\bar{\Omega}$ measurement reflects an underlying mixed population and φ_i are the quantum yields of each species. Rearranging for the individual polarization ratios, we find

$$\Omega_1 = \frac{\sigma_1^{circ}}{\sigma_1^{lin}} = \bar{\Omega}\left(1 + \frac{\gamma_2\sigma_2^{lin}\varphi_2}{\gamma_1\sigma_1^{lin}\varphi_1}\right) - \frac{\gamma_2\sigma_2^{circ}\varphi_2}{\gamma_1\sigma_1^{lin}\varphi_1} \quad (11)$$

$$\Omega_2 = \frac{\sigma_2^{circ}}{\sigma_2^{lin}} = \bar{\Omega}\left(1 + \frac{\gamma_1\sigma_1^{lin}\varphi_1}{\gamma_2\sigma_2^{lin}\varphi_2}\right) - \frac{\gamma_1\sigma_1^{circ}\varphi_1}{\gamma_2\sigma_2^{lin}\varphi_2} \quad (12)$$

Therefore, in addition to $\bar{\Omega}$, determining Ω_1 and Ω_2 would require knowledge of the relative ground state abundances of each species, their polarization dependent 2PA cross sections and their quantum yields. However, we now show that this can also be achieved by combining ensemble polarized 2PA measurements with the parameters describing the fluorescence decays of a heterogeneous population for each excitation condition. These will have the form of eqs 8 and 9 for a two-component system such as NAD(P)H, which can be written in terms of the peak fluorescence intensities $I_{circ}(0)$ and $I_{lin}(0)$ by

$$I_{circ}(t) = I_{circ}(0)[\alpha_1^{circ}\exp(-t/\tau_1) + \alpha_2^{circ}\exp(-t/\tau_2)] \quad (13)$$

$$I_{lin}(t) = I_{lin}(0)[\alpha_1^{lin}\exp(-t/\tau_1) + \alpha_2^{lin}\exp(-t/\tau_2)] \quad (14)$$

where $\alpha_1 + \alpha_2 = 1$. Equating the pre-exponential factors with eqs 8 and 9 gives

$$\alpha_1^{circ} = \frac{A_{circ}\gamma_1\sigma_1^{circ}k_1^{rad}}{I_{circ}(0)} \quad (15)$$

$$\alpha_2^{circ} = \frac{A_{circ}\gamma_2\sigma_2^{circ}k_2^{rad}}{I_{circ}(0)} \quad (16)$$

$$\alpha_1^{lin} = \frac{A_{lin}\gamma_1\sigma_1^{lin}k_1^{rad}}{I_{lin}(0)} \quad (17)$$

$$\alpha_2^{lin} = \frac{A_{lin}\gamma_2\sigma_2^{lin}k_2^{rad}}{I_{lin}(0)} \quad (18)$$

Least squares fits to the intensity decay data yield values for the lifetimes τ_i and amplitudes α_i. The constituent 2PA polarization ratios are then given by

$$\Omega_1 = \frac{\sigma_1^{circ}}{\sigma_1^{lin}} = \frac{I_{circ}(0)}{I_{lin}(0)}\frac{\alpha_1^{circ}}{\alpha_1^{lin}}\frac{A_{lin}}{A_{circ}} \quad (19)$$

$$\Omega_2 = \frac{\sigma_2^{circ}}{\sigma_2^{lin}} = \frac{I_{circ}(0)}{I_{lin}(0)}\frac{\alpha_2^{circ}}{\alpha_2^{lin}}\frac{A_{lin}}{A_{circ}} \quad (20)$$

Integrating eqs 8, 9, 13, and 14 to obtain the total fluorescence emission yields

$$\int_0^\infty I_{circ}(t)\,dt = A_{circ}[\gamma_1\sigma_1^{circ}\varphi_1 + \gamma_2\sigma_2^{circ}\varphi_2] = I_{circ}(0)[\alpha_1^{circ}\tau_1 + \alpha_2^{circ}\tau_2] \quad (21)$$

$$\int_0^\infty I_{lin}(t)\,dt = A_{lin}[\gamma_1\sigma_1^{lin}\varphi_1 + \gamma_2\sigma_2^{lin}\varphi_2] = I_{lin}(0)[\alpha_1^{lin}\tau_1 + \alpha_2^{lin}\tau_2] \quad (22)$$

Dividing eq 21 by eq 22 then gives

$$\frac{\int_0^\infty I_{circ}(t)\,dt}{\int_0^\infty I_{lin}(t)\,dt} = \frac{A_{circ}[\gamma_1\sigma_1^{circ}\varphi_1 + \gamma_2\sigma_2^{circ}\varphi_2]}{A_{lin}[\gamma_1\sigma_1^{lin}\varphi_1 + \gamma_2\sigma_2^{lin}\varphi_2]} = \frac{I_{circ}(0)[\alpha_1^{circ}\tau_1 + \alpha_2^{circ}\tau_2]}{I_{lin}(0)[\alpha_1^{lin}\tau_1 + \alpha_2^{lin}\tau_2]} \quad (23)$$

Substituting eq 10 and rearranging, we obtain

$$\frac{A_{lin}}{A_{circ}} = \frac{I_{lin}(0)}{I_{circ}(0)}\left[\frac{\alpha_1^{lin}\tau_1 + \alpha_2^{lin}\tau_2}{\alpha_1^{circ}\tau_1 + \alpha_2^{circ}\tau_2}\right]\bar{\Omega} \quad (24)$$

Substituting for A_{lin}/A_{circ} in eqs 19 and 20 then gives

$$\Omega_1 = \frac{\alpha_1^{circ}}{\alpha_1^{lin}}\left[\frac{\alpha_1^{lin}\tau_1 + \alpha_2^{lin}\tau_2}{\alpha_1^{circ}\tau_1 + \alpha_2^{circ}\tau_2}\right]\bar{\Omega} \quad (25)$$

$$\Omega_2 = \frac{\alpha_2^{circ}}{\alpha_2^{lin}}\left[\frac{\alpha_1^{lin}\tau_1 + \alpha_2^{lin}\tau_2}{\alpha_1^{circ}\tau_1 + \alpha_2^{circ}\tau_2}\right]\bar{\Omega} \quad (26)$$

These expressions thus allow the Ω values of the subpopulations to be determined by combining the fluorescence decay parameters with the conventional steady state $\bar{\Omega}$ measurement. Our use of this approach to determine the underlying transition tensor structures of the 2PA processes that give rise to the biexponential fluorescence decay of NAD(P)H constitutes the first application of this method.

EXPERIMENTAL METHODS

NAD(P)H Solutions. NADH (N8129, Sigma-Aldrich, Dorset, U.K.) and NADPH (N7505, Sigma-Aldrich, Dorset,

DOI: 10.1021/acs.jpcb.9b01236
J. Phys. Chem. B 2019, 123, 4705−4717

U.K.) were made up fresh on the day of experiment as 1 mM solutions in Milli-Q water containing 10 mM HEPES (H3375, Sigma-Aldrich, Dorset, U.K.) adjusted to pH 7.2.

Laser Sources. For experiments with incident wavelengths between 625 and 720 nm, excitation was provided by the output of an optical parametric amplifier (OPA 9400, Coherent, Cambridgeshire, U.K.) pumped by a regeneratively amplified Ti:sapphire laser (Mira 900F and RegA 9000, Coherent, Cambridgeshire, U.K.) operating at 800 nm with a repetition rate of 250 kHz. For wavelengths between 700 and 780 nm, the 76 MHz output of a Ti:sapphire laser (Mira 900F, Coherent, Cambridgeshire, U.K.) was pulse picked to a repetition rate of 3.8 MHz (PulseSelect, APE, Berlin, Germany) for compatibility with the detection electronics. The 360 nm excitation was obtained by frequency doubling the pulse-picked Ti:sapphire output when tuned to 720 nm using a β-barium borate (BBO) crystal.

Fluorescence Measurements. Both time-dependent and time-averaged polarized fluorescence measurements were made using a modular time correlated single photon counting (TCSPC) system (Ortec, Berkshire, U.K.) described previously.[10] The incident illumination was passed through a Glan-Laser polarizer (Melles-Griot, New York) to ensure vertical polarization and a 25 mm focal length achromatic doublet lens (Melles-Griot, New York) was used to focus the beam onto the sample, held in a 3 mm path length, 50 μL quartz cuvette (Hellma, Essex, U.K.). Fluorescence was collected in a 90° excitation-detection geometry using a 25 cm focal length lens and focused into a multichannel plate photomultiplier tube (MCP-PMT, R3809U, Hamamatsu Photonics, Hertfordshire, U.K.) with a ~100 ps instrument response, passing through a 600 nm short pass filter, to eliminate laser breakthrough, and an emission polarizer. This was set to the appropriate magic angle for absolute fluorescence intensity measurements, recorded from the count rate display of the TCSPC system. For time-resolved fluorescence measurements, a stepper motor rotated the emission polarizer every 10 s to alternately transmit light polarized parallel or perpendicular to the symmetry axis of the excitation polarization (vertical for linear, horizontal for circular). The corresponding decays $I_{\parallel}(t)$ and $I_{\perp}(t)$, spread across 512 channels covering 27 ns, were stored separately in computer memory. Emission events were registered for approximately 60 min for each set of measurements, resulting in a total number of photons collected on the order of 10^5–10^6, well below the 1 in 100 threshold for avoiding pulse pile-up effects.[41]

Two-Photon Action Cross Section Measurements. Following the approach of Xu and Webb,[42] two-photon excitation of a sample by a pulsed laser source of wavelength λ results in a time-averaged total fluorescence intensity of

$$\langle I(t)\rangle = \frac{4}{\pi}\left(\frac{g_p}{fw\lambda}\right) nC\varphi\varepsilon\sigma_{2p}\langle P(t)\rangle^2 \tag{27}$$

where the fluorophore is present at a concentration C in a medium of refractive index n. $\langle P(t)\rangle$ is the time-averaged on-sample power of the illumination pulses with repetition rate f and g_p is a dimensionless quantity dependent on the temporal profile of the laser pulses of duration (fwhm) w. ε quantifies the fraction of the total fluorescence emitted by the fluorophore that is collected, taking into account emission filtering and the spectral efficiency of the detector. The product of the two-photon cross section σ_{2p} and the quantum yield φ is the effective cross section for two-photon excited fluorescence, often referred to as the two-photon action cross section. This is frequently quoted in the units of Goeppert-Mayer (GM) where 1 GM is 10^{-50} cm^4 s photon^{-1}. The two-photon action cross sections of NADH and NADPH solutions could therefore be obtained by comparing the fluorescence intensity emitted at each excitation wavelength with that of reference standards with well characterized 2PA spectra:[42] *p*-bis(*O*-methylstyryl)-benzene (bis-MSB, 15090, Sigma-Aldrich, Dorset, U.K.) in cyclohexane (227048, Sigma-Aldrich, Dorset, U.K.) covering 625 to 740 nm, and rhodamine B (LC6100, Lamdba Physik, Goettingen, Germany) in methanol (154903, Sigma-Aldrich, Dorset, U.K.) covering 700 to 780 nm. The bis-MSB reference spectrum was obtained by combining the relative spectrum provided by Kennedy et al.[43] with the absolute cross section of 69 GM at 585 nm reported by Fisher et al.[44] For rhodamine B, two-photon action cross sections were obtained online from the Zipfel lab at Cornell University.[45] By rearranging eq 27, assuming all incident laser properties remained constant between the reference and NAD(P)H measurements, the two-photon action cross sections could be calculated from

$$(\sigma_{2p}\varphi)_{NAD(P)H} = (\sigma_{2p}\varphi)_{ref}\frac{(nC\varepsilon)_{ref}}{(nC\varepsilon)_{NAD(P)H}}\frac{\langle I_{NAD(P)H}(t)\rangle}{\langle I_{ref}(t)\rangle} \tag{28}$$

Solvent refractive indices n were obtained from the literature.[46,47] Concentrations C were determined using published extinction coefficients[48−50] and a USB spectrometer (USB4000, OceanOptics, Florida, USA) coupled to a xenon white light source. Rhodamine B and bis-MSB solutions were on the order of 10^{-5} M and 10^{-4} M respectively. The parameter ε was calculated as

$$\varepsilon = \int_{\lambda_{min}}^{\lambda_{max}} E(\lambda)F(\lambda)G(\lambda)\,d\lambda \Big/ \int_{\lambda_{min}}^{\lambda_{max}} E(\lambda)\,d\lambda \tag{29}$$

where $E(\lambda)$ is the emission spectrum of the fluorophore obtained from the literature.[51−53] $F(\lambda)$ is the transmission ratio through the 600 nm short-pass emission filter measured using the absorption spectrometer described above. $G(\lambda)$ is the detection efficiency of the MCP-PMT at emission wavelength λ, provided by the manufacturer. Values of $\varepsilon_{NAD(P)H}$ = 0.0751(±0.0003), $\varepsilon_{bis\text{-}MSB}$ = 0.0511(±0.0003), and ε_{RhB} = 0.0249(±0.0001) were determined.

Action cross sections were obtained between 625 and 780 nm at 5 nm intervals. Values at wavelengths with multiple measurements (due to both reference samples being applicable or in the overlap between laser sources) are reported as uncertainty-weighted averages.

Polarized Two-Photon Excitation. The excitation polarization was varied between linear and circular by introducing a zero-order tunable quarter wave plate (Alphalas, Goettingen, Germany) prior to the focusing lens. Circular polarization was confirmed by observing that the power transmitted through a linear analyzing polarizer remained constant throughout its 360° rotation. Measurements of the fluorescence intensity were taken for each polarization in turn, with the emission polarizer set to the corresponding magic angle (54.7° and 35.3° from the vertical for linear and circular polarization respectively). Five $\langle I_{circ}(t)\rangle/\langle I_{lin}(t)\rangle$ pairs were taken at each wavelength, with $\bar{\Omega}$ reported as the mean of these five ratios.

DOI: 10.1021/acs.jpcb.9b01236
J. Phys. Chem. B 2019, 123, 4705−4717

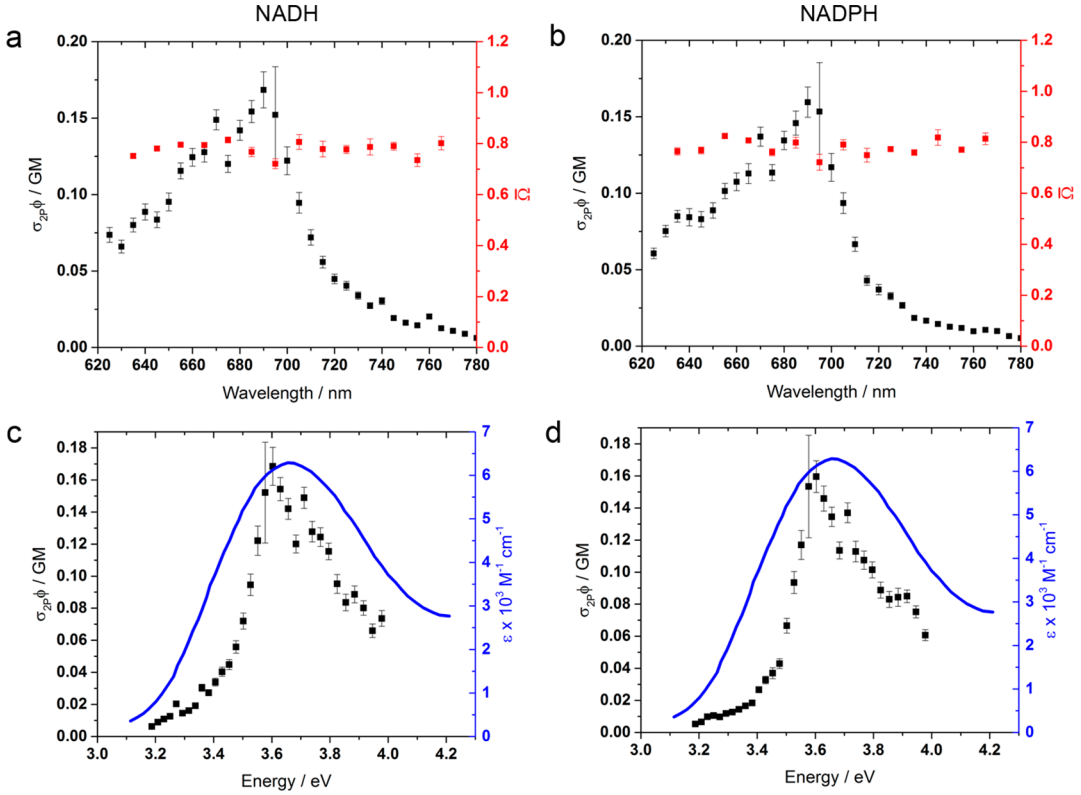

Figure 2. Two-photon action cross section spectra and absorption polarization ratios of (a) NADH and (b) NADPH in aqueous HEPES buffer. No differences in the 2PA absorption characteristics of NADH and NADPH were evident, including in their relative susceptibility to circularly and linearly polarized excitation which remained invariant to excitation wavelength across the two-photon resonance, averaging 0.776(±0.002). The two-photon action cross sections peak at 690 nm at a value of 0.15 GM. This occurs at a similar energy to the 1PA spectrum[50,58] (c and d).

Fluorescence Intensity Decays. Fluorescence decay curves were constructed from the polarized decays $I_{\parallel}(t)$ and $I_{\perp}(t)$ using

$$I(t) = I_{\parallel}(t) + 2I_{\perp}(t) \tag{30}$$

Fluorescence lifetimes were extracted from the $I(t)$ data sets using weighted least-squares tail fitting in OriginPro 2015 (OriginLab, Massachusetts, USA). Goodness-of-fit was determined using the reduced χ^2 parameter

$$\chi_R^{\,2} = \frac{1}{n-l}\sum_{k=1}^{n}\frac{1}{\sigma_k^2}[I_{\text{measured}}(t_k) - I_{\text{model}}(t_k)]^2 \tag{31}$$

where n is the total number of time bins, l is the number of freely varying parameters in the model and $I_{\text{measured}}(t_k)$ and $I_{\text{model}}(t_k)$ are the values of the fluorescence decay data set and model at the time after excitation corresponding to bin k. As $I_{\parallel}(t)$ and $I_{\perp}(t)$ constitute separate Poisson processes with standard deviations $\sqrt{I_{\parallel}(t)}$ and $\sqrt{I_{\perp}(t)}$ respectively, the fit weighting function can be obtained by propagation of uncertainty through eq 30, giving

$$\frac{1}{\sigma_k^{\,2}} = \frac{1}{I_{\parallel}(t_k) + 4I_{\perp}(t_k)} \tag{32}$$

For each time-resolved intensity measurement, a monoexponential fluorescence decay was a poor fit for the data, resulting in $\chi_R^{\,2}$ values of 33(±9). Addition of a second component improved this to a satisfactory 1.55(±0.07), with a triexponential model improving this value no further. All intensity decays were thus well described by biexponential functions as in eqs 8, 9, 13, and 14. The fraction of the total fluorescence emitted by each species i is then given by

$$f_i = \frac{\int_{\infty}\alpha_i \exp(-t/\tau_i)\,dt}{\int_{\infty}[\alpha_1\exp(-t/\tau_1) + \alpha_2\exp(-t/\tau_2)]\,dt} = \frac{\alpha_i\tau_i}{\alpha_1\tau_1 + (1-\alpha_1)\tau_2} \tag{33}$$

Time-Resolved Fluorescence Anisotropy. Anisotropy decays $R(t)$ were constructed from $I_{\parallel}(t)$ and $I_{\perp}(t)$ according to

$$R(t) = \frac{I_{\parallel}(t) - I_{\perp}(t)}{I_{\parallel}(t) + 2I_{\perp}(t)} \tag{34}$$

Anisotropy decay fitting was carried out in OriginPro 2015 using the corresponding weighting function[10]

$$\frac{1}{\sigma_k^{\,2}} = \frac{I(t_k)^2}{[I_{\parallel}(t_k) + 4I_{\perp}(t_k)]R(t_k)^2 - 2[I_{\parallel}(t_k) - 2I_{\perp}(t_k)]R(t_k) + I_{\parallel}(t_k) + I_{\perp}(t_k)} \tag{35}$$

DOI: 10.1021/acs.jpcb.9b01236
J. Phys. Chem. B 2019, 123, 4705−4717

In a two-species system such as NAD(P)H, the observed fluorescence anisotropy is given by the time-dependent weighted average of the component anisotropies, known as the associated anisotropy[54]

$$R(t) = \frac{\alpha_1 R_1(0)\exp(-t/\tau_1)\exp(-t/\tau_1^{rot}) + (1-\alpha_1)R_2(0)\exp(-t/\tau_2)\exp(-t/\tau_2^{rot})}{\alpha_1\exp(-t/\tau_1) + (1-\alpha_1)\exp(-t/\tau_2)} \quad (36)$$

where $R_1(0)$ and $R_2(0)$ are the initial anisotropies of the two subpopulations and τ_1^{rot} and τ_2^{rot} are their rotational correlation times.[10] However, in this work, the time-resolved fluorescence anisotropies of NADH and NADPH arising from both linear and circularly polarized 2PA were suitably fit by a monoexponential decay

$$R_{lin/circ}(t) = R_{lin/circ}(0)\exp(-t/\tau_{lin/circ}^{rot}) \quad (37)$$

with average χ_R^2 values of 1.46(±0.07). χ_R^2 improved no further by increasing the complexity of the fitting function, indicating equal initial anisotropies and rotational correlation times in the two subpopulations, to within experimental uncertainties.

Transition Tensor Structure. Equations 4−7 were solved by using a Monte Carlo method in MATLAB (MathWorks, Massachusetts, USA). The measured $R_{lin}(0)$, $R_{circ}(0)$, $R_{1P}(0)$ and Ω_i were input alongside their uncertainties, defining the mean values and standard deviations of normal distributions of each parameter. Parameter values were picked at random from these four distributions using the normrnd() function and the equations were solved for this set of parameters using fsolve(). This was repeated 10,000 times, with the means and standard deviations of the S and D distributions obtained taken as the solution and its associated uncertainty. 2D polar plots of the tensor structures were constructed by expressing $\underline{\mathbf{S}}$ in 2D polar coordinates

$$A(\theta) = \cos^2\theta + 2D\sin\theta\cos\theta + S\sin^2\theta \quad (38)$$

Error bounds were added to the polar plots by numerical propagation of error through eq 38 in MATLAB.

RESULTS

Two-Photon Absorption Spectra. Wavelengths ranging from 700 to 780 nm have been used to interrogate NAD(P)H in living tissues,[15,55] but its 2PA spectrum has never been fully determined below the Ti:sapphire tuning limit.[18,56,57] Using an optical parametric amplifier (OPA) to bypass this threshold, we measured the two-photon action cross section spectra of NADH and NADPH to be identical, peaking at 690 nm with a value of 0.15(±0.01) GM (see Figure 2). Without explicit knowledge of the relative ground state abundances γ_i, it is not possible to determine the individual two-photon cross sections of the subpopulations of NADH and NADPH. The values of the action cross sections reported here therefore represent an ensemble average. While the peak transition energy in both molecules was similar to that of 1PA, maximized at 340 nm,[58] the two-photon resonance was narrower (fwhm 0.45 vs 0.72 eV), as previously predicted for molecules in the C_s point group[59] to which nicotinamide belongs.[60] The parameter $\bar{\Omega}$ remained constant across the range of excitation wavelengths measured and was identical in NADH and NADPH, with a mean value of 0.787(±0.002). This is consistent with recent Ω measurements on NADH which assumed a homogeneous population[61] and emphasizes the lack of influence over the excited state photophysics of the nicotinamide chromophore by the distant phosphate group that differentiates between the two cofactors.

In both NADH and NADPH, single- and two-photon excitation resulted in similar lifetimes for the two fluorescence decay components, in accordance with Kasha's rule,[62] with average values of 0.362(±0.001) and 0.750(±0.006) ns (see Figure 3 and Table 1). Importantly, while linearly polarized excitation with both single- and two-photon absorption caused 84(±2)% of the short lifetime species to be excited, circularly polarized 2PA resulted in a significantly smaller proportion of the short lifetime state, at 78(±1)%. The individual polarization ratios Ω_i were calculated using eqs 25 and 26, giving values of Ω_1 and Ω_2 that lie below and above $\bar{\Omega}$ respectively. Averaging across the absorption spectrum yielded 0.73(±0.02) and 1.08(±0.07) for NADH with 0.76(±0.04) and 1.07(±0.09) for NADPH. This indicated that the two-photon transitions leading to emission from the short and longer lived states in these molecules have fundamentally different transition tensor structures.

Polarization-Dependent 2P Excitation Spectra. For the heterogeneous populations encountered in NAD(P)H, the 2PA cross section measured here will be a weighted average of the individual cross sections of the two species. Under these conditions, the steady state fluorescence intensity at each excitation wavelength can be related to the constituent concentrations $C_1 = C\gamma_1$ and $C_2 = C\gamma_2$ using eq 27 according to

$$\langle I_\lambda(t)\rangle = \frac{4}{\pi}\left(\frac{g_p}{fw\lambda}\right)n\varepsilon\langle P(t)\rangle^2 C[\gamma_1\varphi_1\sigma_1 + \gamma_2\varphi_2\sigma_2] \quad (39)$$

We assume a common radiative decay rate k_{rad} for both species[10]

$$\langle I_\lambda(t)\rangle = K[\gamma_1\tau_1\sigma_1 + \gamma_2\tau_2\sigma_2] = \langle I_\lambda(t)\rangle_1 + \langle I_\lambda(t)\rangle_2 \quad (40)$$

where

$$K = k_{rad}\frac{4}{\pi}\left(\frac{g_p}{fw\lambda}\right)n\varepsilon\langle P(t)\rangle^2 C \quad (41)$$

From the fluorescence decay dynamics (eqs 17 and 18) we know that the normalized pre-exponential factors are given by

$$\alpha_1 = k\gamma_1\sigma_1 \quad (42)$$

$$\alpha_2 = k\gamma_2\sigma_2 \quad (43)$$

where k is a constant of proportionality. Using eq 33, we can write

$$\langle I_\lambda(t)\rangle_1 = \langle I_\lambda(t)\rangle\frac{\alpha_1\tau_1}{\alpha_1\tau_1 + \alpha_2\tau_2} \quad (44)$$

$$\langle I_\lambda(t)\rangle_2 = \langle I_\lambda(t)\rangle\frac{\alpha_2\tau_2}{\alpha_1\tau_1 + \alpha_2\tau_2} \quad (45)$$

Then, in terms of circular and linear polarizations, we have

DOI: 10.1021/acs.jpcb.9b01236
J. Phys. Chem. B 2019, 123, 4705−4717

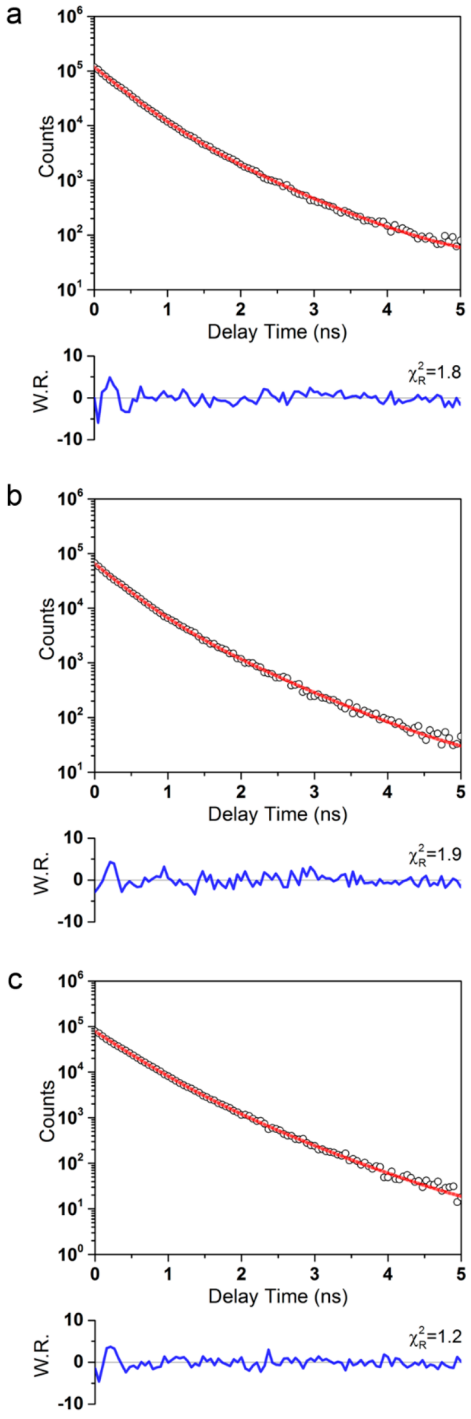

Figure 3. Representative fluorescence intensity decays of 1 mM NADH in aqueous solution excited at 705 nm using (a) linearly polarized 2PA, (b) circularly polarized 2PA, and (c) 1PA at 360 nm excitation. Weighted residuals (W.R.) are the ratio of the difference between the model and the data and the expected standard deviation, calculated using eq 32.

$$\langle I_\lambda(t)\rangle_1^{\text{lin}} = \langle I_\lambda(t)\rangle^{\text{lin}} \frac{{\alpha_1}^{\text{lin}}\tau_1}{{\alpha_1}^{\text{lin}}\tau_1 + {\alpha_2}^{\text{lin}}\tau_2} \tag{46}$$

$$\langle I_\lambda(t)\rangle_2^{\text{lin}} = \langle I_\lambda(t)\rangle^{\text{lin}} \frac{{\alpha_2}^{\text{lin}}\tau_2}{{\alpha_1}^{\text{lin}}\tau_1 + {\alpha_2}^{\text{lin}}\tau_2} \tag{47}$$

$$\langle I_\lambda(t)\rangle_1^{\text{circ}} = \Omega_1\langle I_\lambda(t)\rangle^{\text{lin}} \frac{{\alpha_1}^{\text{lin}}\tau_1}{{\alpha_1}^{\text{lin}}\tau_1 + {\alpha_2}^{\text{lin}}\tau_2} \tag{48}$$

$$\langle I_\lambda(t)\rangle_2^{\text{circ}} = \Omega_2\langle I_\lambda(t)\rangle^{\text{lin}} \frac{{\alpha_2}^{\text{lin}}\tau_2}{{\alpha_1}^{\text{lin}}\tau_1 + {\alpha_2}^{\text{lin}}\tau_2} \tag{49}$$

These quantities are plotted in Figure 4, where it can be seen that, in both NADH and NADPH, the highest intensity emission is observed with linearly polarized excitation of the short lifetime species. In contrast, the longer lifetime state displays similar emission intensities with circular and linear polarized two-photon excitation. This again implies differences in the 2PA tensor structures of the two species; circular polarization favors off-diagonal elements, requiring simultaneous action by the applied electric field along two orthogonal axes, whereas linear polarization favors diagonal transition terms, corresponding to two parallel transition moments requiring simultaneous action twice along a single symmetry axis.[22]

Individual Transition Tensor Structures. The initial single-photon fluorescence anisotropies in NADH and NADPH were found to be 0.36(±0.07) and 0.35(±0.05) respectively, corresponding to transition dipole moment angles θ_M of 20(±10)° for NADH and 16(±9)° for NADPH (see Figure 5 and Table 2). Averaged across all excitation wavelengths, the initial anisotropies following linearly and circularly polarized two-photon absorption of NADH were 0.52(±0.02) and −0.24(±0.03). For NADPH, the corresponding values were 0.55(±0.05) and −0.25(±0.04). The circularly polarized rotational correlation times for NADH of 0.253(±0.002) and NADPH of 0.304(±0.005) ns were faster than the corresponding linearly polarized measurements of 0.323(±0.002) and 0.336(±0.003) ns. Differences between linear and circularly polarized fluorescence anisotropy decay times in a homogeneous population can be indicative of the presence of off-diagonal transition tensor elements.[26,27] Treating NADH and NADPH as a homogeneous systems (using $\bar{\Omega}$) and solving eqs 4−7 suggested a primarily single element tensor, as shown in Table 3. However, when one solved for the tensor elements with the separate values of Ω_1 and Ω_2, differences in 2PA between the two species became apparent. Specifically, in both NADH and NADPH, while the short lifetime state was dominated by a single element, the longer lifetime state contained a significant negative diagonal element averaging $S = -0.32(\pm 0.04)$. Polar plots of the 2PA tensors[63] of the two species are shown in Figure 6, which demonstrates that the effect of the negative value of S in the longer lifetime species is the presence of distinct negative amplitude lobes in the polar plot and a rotation of the principal axis of the tensor. The angle of rotation is calculated by differentiating eq 38 to find the turning point

$$\left(\frac{\partial A}{\partial \theta}\right)_{\theta=\theta_{\text{turn}}} = 2D\cos 2\theta_{\text{turn}} + (S-1)\sin 2\theta_{\text{turn}} = 0 \tag{50}$$

$$\theta_{\text{turn}} = \frac{1}{2}\arctan\left(\frac{2D}{1-S}\right) \tag{51}$$

The combined values in Table 3 imply $\theta_{\text{turn}} = 3(\pm 4)°$ for the long lifetime species.

DOI: 10.1021/acs.jpcb.9b01236
J. Phys. Chem. B 2019, 123, 4705−4717

Table 1. Biexponential Fitting Parameters of Fluorescence Intensity Decays of NADH and NADPH in Aqueous Buffer, across the Tuning Spectrum of the Ti:Sapphire Laser and with Single-Photon Excitation at 360 nm for Comparison

		linear			circular		
	λ/nm	α_1	τ_1/ns	τ_2/ns	α_1	τ_1/ns	τ_2/ns
NADH	705	0.73(±0.06)	0.344(±0.009)	0.69(±0.02)	0.69(±0.05)	0.315(±0.007)	0.70(±0.01)
	715	0.86(±0.06)	0.367(±0.009)	0.93(±0.08)	0.78(±0.09)	0.34(±0.02)	0.79(±0.06)
	725	0.86(±0.02)	0.380(±0.004)	0.78(±0.01)	0.72(±0.03)	0.330(±0.005)	0.68(±0.01)
	735	0.83(±0.02)	0.366(±0.004)	0.77(±0.01)	0.78(±0.03)	0.350(±0.005)	0.76(±0.01)
	745	0.82(±0.02)	0.378(±0.004)	0.78(±0.01)	0.86(±0.03)	0.391(±0.004)	0.84(±0.02)
	755	0.87(±0.03)	0.395(±0.005)	0.84(±0.03)	0.80(±0.03)	0.357(±0.006)	0.78(±0.02)
	765	0.88(±0.02)	0.396(±0.004)	0.90(±0.03)	0.82(±0.03)	0.365(±0.005)	0.81(±0.02)
	mean	0.85(±0.01)	0.379(±0.002)	0.78(±0.01)	0.79(±0.01)	0.357(±0.002)	0.74(±0.01)
	360	0.83(±0.02)	0.382(±0.005)	0.72(±0.02)	–	–	–
NADPH	705	0.8(±0.2)	0.41(±0.03)	0.9(±0.1)	0.7(±0.1)	0.27(±0.01)	0.73(±0.01)
	715	0.79(±0.05)	0.349(±0.008)	0.72(±0.02)	0.76(±0.06)	0.321(±0.009)	0.72(±0.02)
	725	0.80(±0.06)	0.36(±0.01)	0.73(±0.03)	0.7(±0.1)	0.29(±0.01)	0.68(±0.02)
	735	0.81(±0.04)	0.354(±0.007)	0.78(±0.02)	0.68(±0.08)	0.285(±0.009)	0.72(±0.02)
	745	0.83(±0.04)	0.373(±0.007)	0.77(±0.02)	0.79(±0.05)	0.327(±0.009)	0.73(±0.02)
	755	0.86(±0.05)	0.40(±0.01)	0.84(±0.05)	0.80(±0.04)	0.348(±0.008)	0.79(±0.02)
	765	0.81(±0.06)	0.37(±0.01)	0.83(±0.03)	0.75(±0.06)	0.319(±0.009)	0.78(±0.02)
	mean	0.82(±0.02)	0.366(±0.003)	0.77(±0.01)	0.76(±0.02)	0.315(±0.003)	0.73(±0.01)
	360	0.85(±0.03)	0.378(±0.006)	0.77(±0.02)	–	–	–
combined	2PA	0.84(±0.01)	0.374(±0.002)	0.78(±0.01)	0.78(±0.01)	0.346(±0.002)	0.73(±0.01)
	1PA	0.84(±0.02)	0.380(±0.004)	0.74(±0.01)	–	–	–

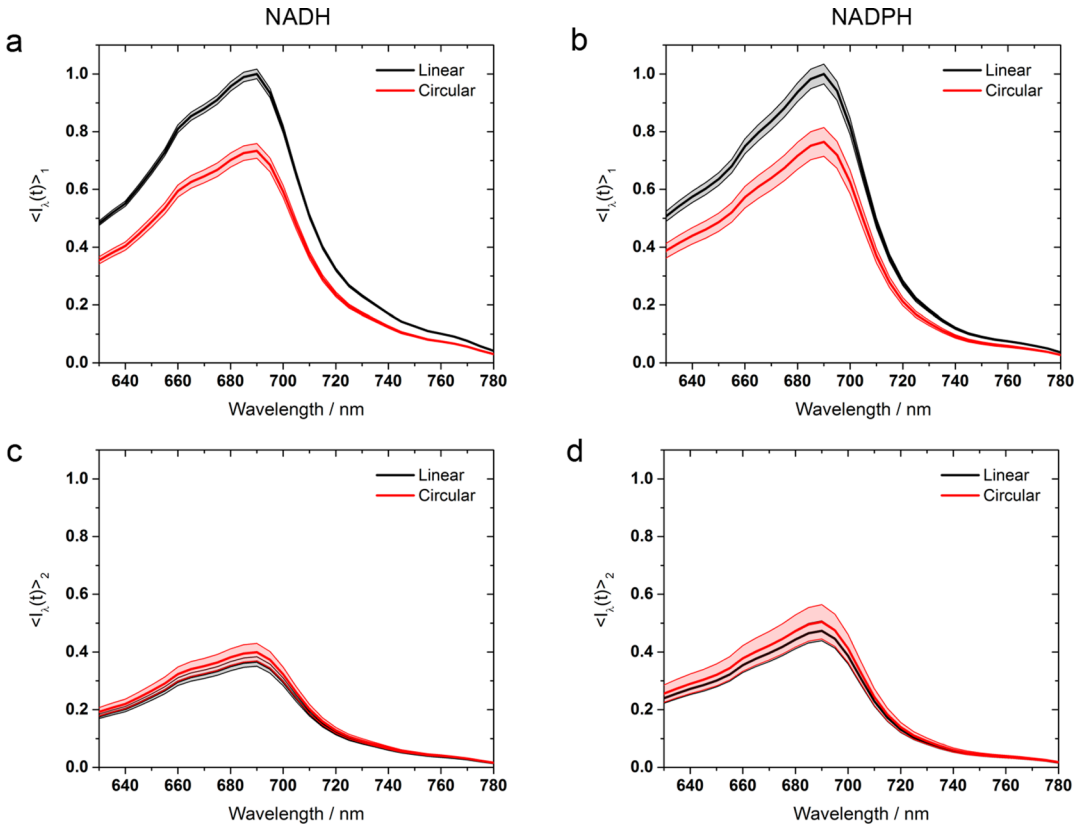

Figure 4. Relative fluorescence intensity of the two NAD(P)H species as a function of excitation wavelength, with the short lifetime linearly polarized peak of each molecule arbitrarily scaled to 1. While the short lifetime species favors linearly polarized excitation in both NADH and NADPH (a and b), the longer lifetime species exhibits similar fluorescence intensities with both excitation polarizations (c and d). Shaded areas represent uncertainty bounds.

DISCUSSION

We have identified clear differences in the structures of the two-photon transitions giving rise to the short and long lifetime fluorescent species of NADH and NADPH. Our work therefore rules out two proposed, but unproven, mechanisms for the heterogeneous intensity decay dynamics observed. Dynamic quenching by the adenine moiety in the folded state

DOI: 10.1021/acs.jpcb.9b01236
J. Phys. Chem. B 2019, 123, 4705−4717

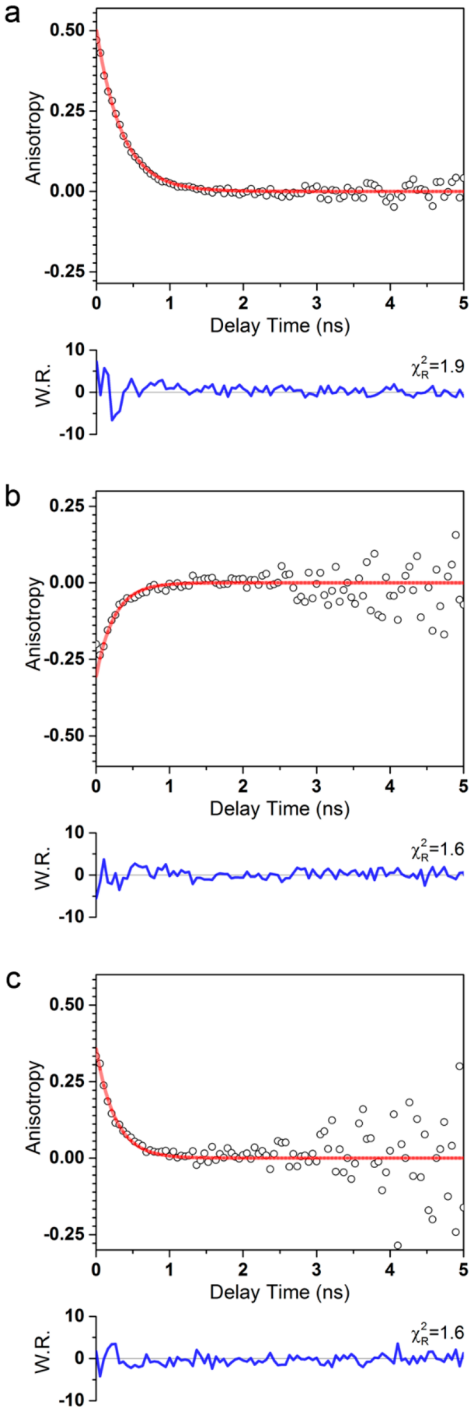

Figure 5. Representative fluorescence anisotropy decays of 1 mM NADH in aqueous solution excited at 705 nm using (a) linearly polarized 2PA, (b) circularly polarized 2PA, and (c) 1PA at 360 nm excitation. Weighted residuals (W.R.) are the ratio of the difference between the model and the data and the expected standard deviation, calculated using eq 35.

has been widely assumed,[14,15] while a kinetic scheme involving a single emitting excited state species with conversion into a nonfluorescent product has also been proposed.[12] As these are both postexcitation phenomena, the 2PA transition would be common to both components, which is clearly not observed here.

Opposing signs of S_{XX} and S_{YY} in the 2PA tensor of the long lifetime NAD(P)H species caused negative lobes that were absent in the short lifetime species. Parallels can be drawn between these results and the behavior of the ^1L_b absorption band of indole.[64,65] Callis[63] observed negative lobes to be present in the 2PA tensor of pure indole, which were then reduced significantly upon the addition of a single methyl group to the pyrole ring. The difference in the 2PA tensors of the short and long lifetime species of NAD(P)H clearly cannot be attributed to differing substituent groups. However, alternate configurations of the nicotinamide ring have previously been suggested to play a role in the spectral properties of the molecule, particularly those involving the amide group.[2,13] Both 1PA and 2PA are predicted to be accompanied by charge transfer from the pyridine ring nitrogen to the oxygen of the amide group,[18] which favors the *cis* conformation displayed in Figure 1.[66] A *trans* conformation, in which the amide group is rotated by 180°, can also be adopted[67] (see Figure 1). The contrasting electronic rearrangement taking place following absorption in each species, due to the differing location of the oxygen atom relative to the ring nitrogen in the two configurations, may then be sufficient to alter the symmetry of the two-photon transition. Enzyme binding sites are known to favor the *trans* conformation of NAD(P)H[67] in addition to altering its local electrostatic environment.[68] It is possible that these effects could also contribute to the photophysical alterations induced by the binding of NADH and NADPH to different enzymes. This will be the subject of future studies.

Quantum chemical calculations have predicted a single element 2PA tensor for the nicotinamide chromophore as we observed in the short lifetime species, with the principal axis collinear to the 1PA transition dipole.[18] These calculations involved a free energy minimization step, so were likely carried out on the *cis* configuration of the amide group as the free energy of the *trans* form is 1 kcal mol^{-1} higher.[67] For a difference in Gibbs free energy ΔG, the relative amounts of each species present at equilibrium are given by[69]

$$\gamma_{cis} = \frac{1}{\exp(-\Delta G/RT) + 1} \tag{52}$$

$$\gamma_{trans} = \frac{1}{\exp(\Delta G/RT) + 1} \tag{53}$$

where R is the universal gas constant and T is the temperature. At a lab temperature of 21 °C, 85% of the NAD(P)H population would be expected to assume the *cis* configuration and 15% the *trans* configuration. These values are in precise agreement with the linearly polarized decay amplitudes we measure here. If the two components in the fluorescence decay of NAD(P)H do indeed correspond to the *cis* and *trans* form of the nicotinamide ring, this would imply $\alpha_1^{lin} = \gamma_{cis} = 0.85$ and $\alpha_2^{lin} = \gamma_{trans} = 0.15$. By eqs 42 and 43, the linearly polarized 2PA cross sections of the two species would therefore be equal, which could explain the absence of characteristic spectral features corresponding to each fluorescent species in the absorption spectra.[2,50,58] The circularly polarized 2PA cross section of the short lifetime species would then be a factor of $\Omega_1 = 0.74$ lower, causing the smaller contribution of this component to the fluorescence decay with circularly polarized two-photon excitation.

Our previous work suggested that the contrasting lifetimes of the two fluorescent species of NAD(P)H arise from differences in the shape of the potential energy surfaces encountered as they undergo nonradiative conformational

DOI: 10.1021/acs.jpcb.9b01236
J. Phys. Chem. B 2019, 123, 4705−4717

Table 2. Fluorescence Anisotropy Decay Parameters of NADH and NADPH in Aqueous Buffer, across the Tuning Spectrum of the Ti:Sapphire Laser and with Single-Photon Excitation at 360 nm for Comparison

		linear		circular	
	λ/nm	$R_L(0)$	τ_L^{rot}/ns	$R_C(0)$	τ_C^{rot}/ns
NADH	705	0.53(±0.07)	0.277(±0.006)	−0.2(±0.1)	0.27(±0.01)
	715	0.5(±0.1)	0.279(±0.005)	−0.28(±0.08)	0.260(±0.007)
	725	0.55(±0.08)	0.290(±0.004)	−0.25(±0.08)	0.264(±0.008)
	735	0.5(±0.1)	0.324(±0.009)	−0.25(±0.08)	0.244(±0.007)
	745	0.50(±0.03)	0.346(±0.002)	−0.23(±0.05)	0.252(±0.004)
	755	0.52(±0.08)	0.323(±0.005)	−0.24(±0.08)	0.246(±0.007)
	765	0.5(±0.1)	0.360(±0.007)	−0.25(±0.08)	0.249(±0.007)
	mean	0.52(±0.02)	0.323(±0.002)	−0.24(±0.03)	0.253(±0.002)
	360	0.36(±0.07)	0.258(±0.006)	–	–
NADPH	705	0.5(±0.3)	0.28(±0.02)	−0.3(±0.1)	0.32(±0.01)
	715	0.5(±0.1)	0.308(±0.008)	−0.2(±0.1)	0.28(±0.01)
	725	0.5(±0.1)	0.364(±0.007)	−0.3(±0.1)	0.35(±0.02)
	735	0.6(±0.1)	0.316(±0.008)	−0.3(±0.1)	0.29(±0.02)
	745	0.6(±0.1)	0.357(±0.007)	−0.25(±0.08)	0.35(±0.01)
	755	0.6(±0.1)	0.338(±0.009)	−0.2(±0.1)	0.30(±0.02)
	765	0.5(±0.2)	0.364(±0.01)	−0.2(±0.2)	0.25(±0.01)
	mean	0.55(±0.05)	0.336(±0.003)	−0.25(±0.04)	0.304(±0.005)
	360	0.35(±0.05)	0.42(±0.01)	–	–
combined	2PA	0.52(±0.02)	–	−0.25(±0.02)	–
	1PA	0.36(±0.04)	–	–	–

Table 3. Tensor Components for the Two Fluorescence Decay Components of NADH and NADPH[a]

	short lifetime species		long lifetime species		homogeneous treatment	
	S	D	S	D	S	D
NADH	−0.06(±0.02)	−0.02(±0.05)	−0.33(±0.05)	0(±0.1)	−0.09(±0.01)	−0.03(±0.05)
NADPH	−0.07(±0.05)	0(±0.1)	−0.29(±0.07)	0.1(±0.2)	−0.07(±0.03)	0(±0.1)
combined	−0.06(±0.02)	0(±0.04)	−0.32(±0.04)	0.1(±0.1)	−0.09(±0.01)	−0.03(±0.05)

[a]In both molecules, the long lifetime species exhibits a significant negative diagonal element, in contrast to the primarily single element short lifetime species. These differences could not be observed if the analysis assumed a homogeneous system. As the tensor components of the two molecules are identical, suggesting that the phosphate group which differentiates between them plays no role in the transition, the datasets were combined to reduce uncertainties before plotting in Figure 6.

relaxation back to the ground state.[10] Specifically, the frequency of the initial potential energy well of short lifetime species was double that of the long lifetime species, leading to a nonradiative rate twice as large. The small magnitudes of the initial well frequencies were consistent with small scale motion for the conformational relaxation, such as the puckering that occurs in the nicotinamide ring.[70] Interestingly, this puckering is known to be altered in the *trans* state,[67] which could lead to the differences in well frequencies and therefore the different lifetimes. Time-resolved fluorescence anisotropy measurements are potentially sensitive to such differences in molecular structure. In the present study, rapid monoexponential anisotropy decay times (approaching the MCP-PMT response) were observed for NAD(P)H. In our previous work,[10] the increased fluorescence intensity afforded by 1PA, together with the enhanced quantum yield and slower (nanosecond) rotational diffusion times of NAD(P)H in more viscous environments, revealed associated (heterogeneous) anisotropy decay dynamics with distinct rotational diffusion times of the two subpopulations. In both NADH and NADPH, the rotational diffusion rates of the long lifetime species were on average 1.9 times lower than those of the short lifetime species. From the Stokes−Einstein−Debye equation, this implies differing form factors or hydrodynamic volumes for the two species.[10] The amide group lies approximately 20° out of the plane of the nicotinamide ring in the *trans* configuration,[67] which could provide a physical basis for these observations.

It had previously been shown[16] that the potential energy barrier encountered by both species during conformational relaxation was equal at 1.5 kcal mol^{-1}. The barrier encountered during the *cis-trans* transition is almost five times larger.[67] Alongside our previous data suggesting that the variation in nonradiative decay rate with viscosity was inconsistent with the internal conversion involving an isomerization,[10] this implies that no switching between the *cis* and *trans* configurations occurs in the excited state dynamics. The heterogeneous fluorescence decay dynamics of NAD(P)H solutions therefore correspond to two distinct ground state species, with separate 2PA transition tensors and dissimilar lifetimes due to different conformational relaxation rates.

CONCLUSIONS

Knowledge of the 2PA polarization ratio Ω has proven to be an invaluable means of determining the 2PA transition tensor and the symmetry of the participating states. Measurement of Ω has, until now, been the preserve of steady state or time-averaged fluorescence intensity measurements. While this is a valid approach in the study of 2PA in homogeneous populations, we have shown that for heterogeneous systems

DOI: 10.1021/acs.jpcb.9b01236
J. Phys. Chem. B 2019, 123, 4705−4717

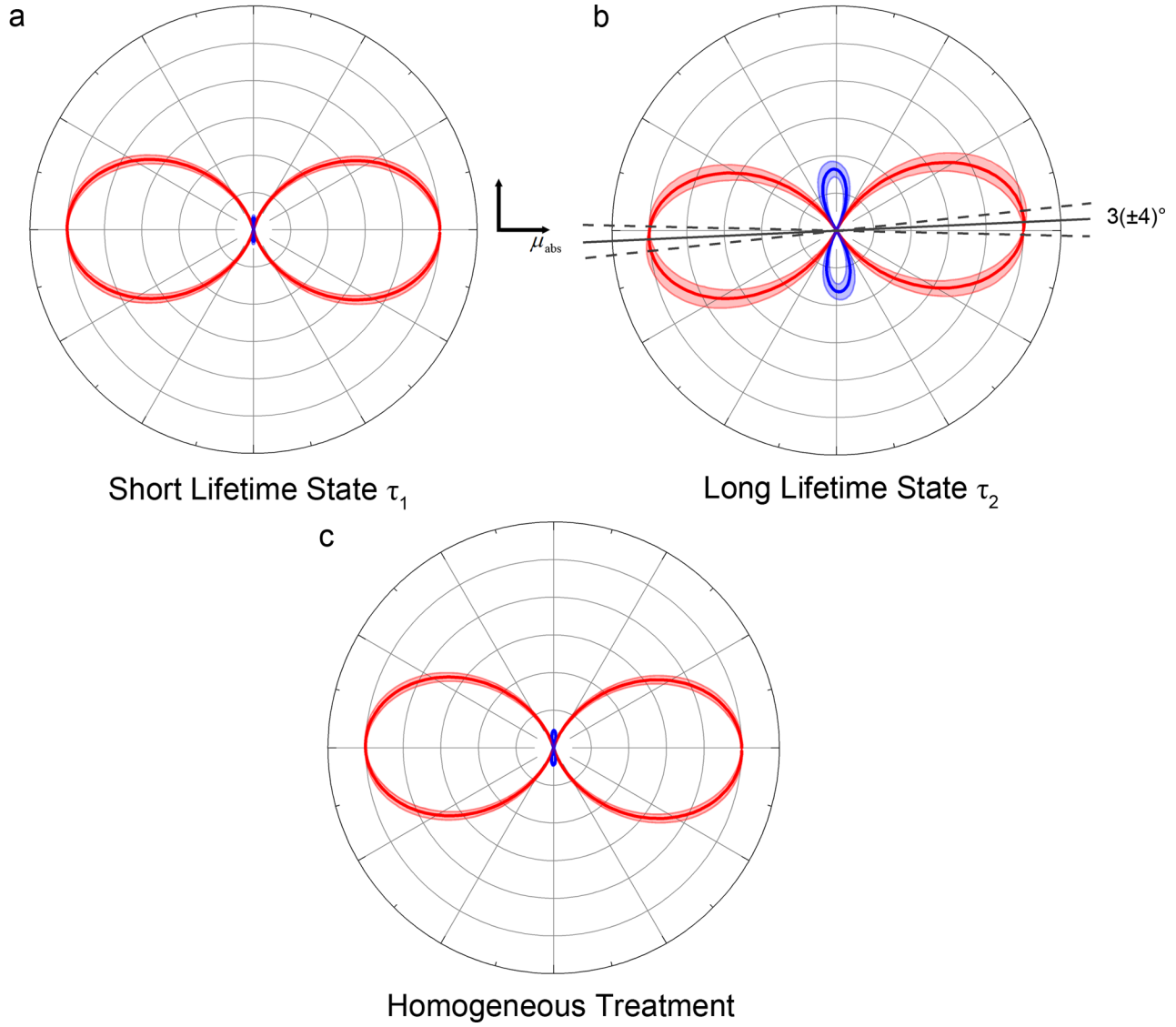

Figure 6. 2PA tensor polar plots for the combined NADH and NADPH data displayed in Table 3. The distance of the line to the origin dictates the transition amplitude at each angle. Red and blue lines indicate positive and negative amplitudes, respectively. Shaded areas represent uncertainty bounds. While the short lifetime tensor is dominated by a single element (a), the long lifetime species exhibits negative lobes which rotate the direction of maximum absorption by around 3° from the single-photon S_0-S_1 transition (b). These features could not be resolved if the excited state population was treated as homogeneous (c).

Ω is related to the constituent 2PA transitions by a ratio of decay amplitudes and lifetimes which steady state measurements cannot provide. The introduction of time-resolved fluorescence measurements is therefore required to extract the individual Ω values of each species. It is then possible to determine the 2D tensor elements of the individual 2PA transitions by introducing linear and circularly polarized fluorescence anisotropy measurements. We have utilized this approach to show, for the first time, that the biexponential fluorescence decay in NAD(P)H arises from two distinct 2PA processes with different transition tensor structures. Our results point to the existence of structural differences in the nicotinamide ring of the two subpopulations as the underlying cause of the observed difference in their nonradiative activated barrier crossing decay rates,[10] and they do not accord with postabsorption mechanisms such as intermolecular quenching or excited state reactions.[12,14,15] An enhanced understanding of NAD(P)H photophysics will assist in promoting its use as an accurate, endogenously fluorescent reporter of intercellular biochemistry.[3−8] The approaches outlined here will also find immediate application in other biological fluorescence studies where heterogeneous populations are known to exist, in particular those involving fluorescent proteins,[71,72] and the state restriction observed in their Förster resonance energy transfer (FRET) dynamics.[25,54,73]

AUTHOR INFORMATION

Corresponding Author

*(A.J.B.) E-mail: a.bain@ucl.ac.uk.

ORCID

Angus J. Bain: 0000-0001-8705-8536

Notes

The authors declare no competing financial interest.

DOI: 10.1021/acs.jpcb.9b01236
J. Phys. Chem. B 2019, 123, 4705−4717

■ ACKNOWLEDGMENTS

This work was funded by BBSRC Grant BB/P018726/1, "New approaches to studying redox metabolism using time-resolved NAD(P)H fluorescence and anisotropy".

■ REFERENCES

(1) Ying, W. NAD+/NADH and NADP+/NADPH in Cellular Functions and Cell Death: Regulation and Biological Consequences. *Antioxid. Redox Signaling* **2008**, *10* (2), 179−206.
(2) De Ruyck, J. J.; Famerée, M.; Wouters, J.; Perpète, E. A.; Preat, J.; Jacquemin, D. Towards the Understanding of the Absorption Spectra of NAD(P)H/NAD(P)+ as a Common Indicator of Dehydrogenase Enzymatic Activity. *Chem. Phys. Lett.* **2007**, *450* (1−3), 119−122.
(3) Blacker, T. S.; Duchen, M. R. Investigating Mitochondrial Redox State Using NADH and NADPH Autofluorescence. *Free Radical Biol. Med.* **2016**, *100*, 53−65.
(4) Horilova, J.; Mateasik, A.; Revilla-i-Domingo, R.; Raible, F.; Chorvat, D., Jr; Chorvatova, A. M. Fingerprinting of Metabolic States by NAD (P) H Fluorescence Lifetime Spectroscopy in Living Cells: A Review. *Med. Photonics* **2015**, *27*, 62−69.
(5) Schaefer, P. M.; Kalinina, S.; Rueck, A.; von Arnim, C. A. F.; von Einem, B. NADH Autofluorescence - A Marker on Its Way to Boost Bioenergetic Research. *Cytometry, Part A* **2019**, *95*, 34−46.
(6) Kolenc, O. I.; Quinn, K. P. Evaluating Cell Metabolism Through Autofluorescence Imaging of NAD (P) H and FAD. *Antioxid. Redox Signaling* **2019**, *30*, 875−889.
(7) Blacker, T. S.; Sewell, M. D. E.; Szabadkai, G.; Duchen, M. R. Metabolic Profiling of Live Cancer Tissues Using NAD (P) H Fluorescence Lifetime Imaging. *Methods Mol. Biol.* **2019**, *1928*, 365−387.
(8) Blacker, T. S.; Duchen, M. R. Characterizing Metabolic States Using Fluorescence Lifetime Imaging Microscopy (FLIM) of NAD(P)H. *Neuromethods* **2017**, *123*, 133−150.
(9) Lee, H. B.; Cong, A.; Leopold, H.; Currie, M.; Boersma, A.; Sheets, E. D.; Heikal, A. A. Rotational and Translational Diffusion of Size-Dependent Fluorescent Probes in Homogeneous and Heterogeneous Environments. *Phys. Chem. Chem. Phys.* **2018**, *20*, 24045−24057.
(10) Blacker, T. S.; Marsh, R. J.; Duchen, M. R.; Bain, A. J. Activated Barrier Crossing Dynamics in the Non-Radiative Decay of NADH and NADPH. *Chem. Phys.* **2013**, *422*, 184−194.
(11) Visser, A. J. W. G.; Hoek, A. v. The Fluorescence Decay of Reduced Nicotinamides in Aqueous Solution after Excitation with a UV-Mode Locked Locked Ar ION Laser. *Photochem. Photobiol.* **1981**, *33* (1), 35−40.
(12) Gafni, A.; Brand, L. Fluorescence Decay Studies of Reduced Nicotinamide Adenine Dinucleotide in Solution and Bound to Liver Alcohol Dehydrogenase. *Biochemistry* **1976**, *15* (15), 3165−3171.
(13) Hull, R. V.; Conger, P. S., 3rd; Hoobler, R. J. Conformation of NADH Studied by Fluorescence Excitation Transfer Spectroscopy. *Biophys. Chem.* **2001**, *90* (1), 9−16.
(14) Ghukasyan, V. V.; Kao, F.-J. Monitoring Cellular Metabolism with Fluorescence Lifetime of Reduced Nicotinamide Adenine Dinucleotide. *J. Phys. Chem. C* **2009**, *113* (27), 11532−11540.
(15) Skala, M. C.; Riching, K. M.; Bird, D. K.; Gendron-Fitzpatrick, A.; Eickhoff, J.; Eliceiri, K. W.; Keely, P. J.; Ramanujam, N. In Vivo Multiphoton Fluorescence Lifetime Imaging of Protein-Bound and Free Nicotinamide Adenine Dinucleotide in Normal and Precancerous Epithelia. *J. Biomed. Opt.* **2007**, *12* (2), 024014.
(16) Couprie, M. E.; Mérola, F.; Tauc, P.; Garzella, D.; Delboulbé, A.; Hara, T.; Billardon, M. First Use of the UV Super-ACO Free-Electron Laser: Fluorescence Decays and Rotational Dynamics of the NADH Coenzyme. *Rev. Sci. Instrum.* **1994**, *65* (5), 1485.
(17) Heiner, Z.; Roland, T.; Leonard, J.; Haacke, S.; Groma, G. I. Kinetics of Light-Induced Intramolecular Energy Transfer in Different Conformational States of NADH. *J. Phys. Chem. B* **2017**, *121* (34), 8037−8045.
(18) Kierdaszuk, B.; Malak, H.; Gryczynski, I.; Callis, P.; Lakowicz, J. R. Fluorescence of Reduced Nicotinamides Using One- and Two-Photon Excitation. *Biophys. Chem.* **1996**, *62* (1−3), 1−13.
(19) Krishnamoorthy, G.; Periasamy, N.; Venkataraman, B. On the Origin of Heterogeneity of Fluorescence Decay Kinetics of Reduced Nicotinamide Adenine Dinucleotide. *Biochem. Biophys. Res. Commun.* **1987**, *144* (1), 387−392.
(20) Brink, D. M.; Satchler, G. R. *Angular Momentum*; Clarendon Press: 1968.
(21) Bray, R. G.; Hochstrasser, R.-M. Two-Photon Absorption by Rotating Diatomic Molecules. *Mol. Phys.* **1976**, *31* (4), 1199−1211.
(22) Bain, A. J. Multiphoton Processes. *Photonics* **2015**, *1*, 279−320.
(23) Drucker, R. P.; McClain, W. M. Polarized Two-Photon Studies of Biphenyl and Several Derivatives. *J. Chem. Phys.* **1974**, *61* (7), 2609−2615.
(24) Wan, C.; Johnson, C. K. Time-Resolved Two-Photon Induced Anisotropy Decay: The Rotational Diffusion Regime. *J. Chem. Phys.* **1994**, *101* (12), 10283.
(25) Masters, T. A.; Marsh, R. J.; Blacker, T. S.; Armoogum, D. A.; Larijani, B.; Bain, A. J. Polarized Two-Photon Photoselection in EGFP: Theory and Experiment. *J. Chem. Phys.* **2018**, *148*, 134311.
(26) Ryderfors, L.; Mukhtar, E.; Johansson, L. B.-A. The Symmetry of Two-Photon Excited States as Determined by Time-Resolved Fluorescence Depolarization Experiments. *J. Phys. Chem. A* **2007**, *111* (45), 11531−11539.
(27) Ryderfors, L.; Mukhtar, E.; Johansson, L. B.-Å. Excited-State Symmetry and Reorientation Dynamics of Perylenes in Liquid Solutions: Time-Resolved Fluorescence Depolarization Studies Using One-and Two-Photon Excitation. *J. Phys. Chem. A* **2008**, *112* (26), 5794−5803.
(28) Callis, P. R. Two-Photon-Induced Fluorescence. *Annu. Rev. Phys. Chem.* **1997**, *48*, 271−297.
(29) Callis, P. R.; Scott, T. W.; Albrecht, A. C. Polarized Two-Photon Fluorescence Excitation Studies of Pyrimidine. *J. Chem. Phys.* **1981**, *75* (12), 5640−5646.
(30) Berg, J. O.; Parker, D. H.; El-Sayed, M. A. Symmetry Assignment of Two-Photon States from Polarization Characteristics of Multiphoton Ionization Spectra. *J. Chem. Phys.* **1978**, *68* (12), 5661−5663.
(31) Scott, T. W.; Albrecht, A. C. A Rydberg Transition in Benzene in the Condensed Phase: Two-Photon Fluorescence Excitation Studies. *J. Chem. Phys.* **1981**, *74* (7), 3807−3812.
(32) Scott, T. W.; Haber, K. S.; Albrecht, A. C. Two-Photon Photoselection in Rigid Solutions: A Study of the B 2 U← A 1 G Transition in Benzene. *J. Chem. Phys.* **1983**, *78* (1), 150−157.
(33) Monson, P. R.; McClain, W. M. Complete Polarization Study of the Two-Photon Absorption of Liquid 1-Chloronaphthalene. *J. Chem. Phys.* **1972**, *56* (10), 4817−4825.
(34) Yu, J.-A.; Nocera, D. G.; Leroi, G. E. Two-Photon Excitation Spectrum of Perylene in Solution. *Chem. Phys. Lett.* **1990**, *167* (1−2), 85−89.
(35) Faidas, H.; Siomos, K. Two-Photon Excitation Spectroscopy of Benzene and Toluene in Nonpolar Liquids. *J. Mol. Spectrosc.* **1988**, *130* (2), 288−302.
(36) Pauls, S. W.; Hedstrom, J. F.; Johnson, C. K. Rotational Relaxation of Perylene in N-Alcohols and N-Alkanes Studied by Two-Photon-Induced Anisotropy Decay. *Chem. Phys.* **1998**, *237* (1), 205−222.
(37) Dick, B.; Gonska, H.; Hohlneicher, G. Two Photon Spectroscopy of Dipole Forbidden Transitions III. Experimental Determination of Two Photon Absorption Spectra Including Polarization Control. *Berichte der Bunsengesellschaft für Phys. Chemie* **1981**, *85* (8), 746−754.
(38) Vivas, M. G.; Diaz, C.; Echevarria, L.; Mendonca, C. R.; Hernández, F. E.; De Boni, L. Two-Photon Circular−Linear Dichroism of Perylene in Solution: A Theoretical−Experimental Study. *J. Phys. Chem. B* **2013**, *117* (9), 2742−2747.

DOI: 10.1021/acs.jpcb.9b01236
J. Phys. Chem. B 2019, 123, 4705−4717

(39) Wirth, M. J.; Koskelo, A. C.; Mohler, C. E. Study of Solvation Symmetry by Two-Photon Polarization Measurements. *J. Phys. Chem.* **1983**, *87* (22), 4395−4400.
(40) Chuang, T. J.; Eisenthal, K. B. Theory of Fluorescence Depolarization by Anisotropic Rotational Diffusion. *J. Chem. Phys.* **1972**, *57* (12), 5094−5097.
(41) Salthammer, T. Numerical Simulation of Pile-up Distorted Time-Correlated Single Photon Counting (TCSPC) Data. *J. Fluoresc.* **1992**, *2* (1), 23−27.
(42) Xu, C.; Webb, W. W. Measurement of Two-Photon Excitation Cross Sections of Molecular Fluorophores with Data from 690 to 1050 Nm. *J. Opt. Soc. Am. B* **1996**, *13* (3), 481−491.
(43) Kennedy, S. M.; Lytle, F. E. P-Bis (O-Methylstyryl) Benzene as a Power-Squared Sensor for Two-Photon Absorption Measurements between 537 and 694 Nm. *Anal. Chem.* **1986**, *58* (13), 2643−2647.
(44) Fisher, W. G.; Wachter, E. A.; Lytle, F. E.; Armas, M.; Seaton, C. Source-Corrected Two-Photon Excited Fluorescence Measurements between 700 and 880 Nm. *Appl. Spectrosc.* **1998**, *52* (4), 536−545.
(45) Zipfel, W. R. https://zipfellab.bme.cornell.edu/cross_sections.html.
(46) Schiebener, P.; Straub, J.; Levelt Sengers, J. M. H.; Gallagher, J. S. Refractive Index of Water and Steam as Function of Wavelength, Temperature and Density. *J. Phys. Chem. Ref. Data* **1990**, *19* (3), 677−717.
(47) Rheims, J.; Köser, J.; Wriedt, T. Refractive-Index Measurements in the near-IR Using an Abbe Refractometer. *Meas. Sci. Technol.* **1997**, *8* (6), 601.
(48) Ding, X.-F.; et al. Measurement of the Fluorescence Quantum Yield of Bis-MSB. *Chin. Phys. C* **2015**, *39* (12), 126001.
(49) Faraggi, M.; Peretz, P.; Rosenthal, I.; Weinraub, D. Solution Properties of Dye Lasers. Rhodamine B in Alcohols. *Chem. Phys. Lett.* **1984**, *103*, 310−314.
(50) Ziegenhorn, J.; Senn, M.; Bücher, T. Molar Absorptivities of Beta-NADH and Beta-NADPH. *Clin. Chem.* **1976**, *22* (2), 151−160.
(51) Du, H.; Fuh, R. C. A.; Li, J.; Corkan, L. A.; Lindsey, J. S. PhotochemCAD: A Computer-Aided Design and Research Tool in Photochemistry. *Photochem. Photobiol.* **1998**, *68* (2), 141−142.
(52) Patterson, G. H.; Knobel, S. M.; Arkhammar, P.; Thastrup, O.; Piston, D. W. Separation of the Glucose-Stimulated Cytoplasmic and Mitochondrial NAD(P)H Responses in Pancreatic Islet Beta Cells. *Proc. Natl. Acad. Sci. U. S. A.* **2000**, *97* (10), 5203−5207.
(53) Lakowicz, J. R.; Gryczynski, I. Characterization of P-Bis (O-Methylstyryl) Benzene as a Lifetime and Anisotropy Decay Standard for Two-Photon Induced Fluorescence. *Biophys. Chem.* **1993**, *47* (1), 1−7.
(54) Blacker, T. S.; Chen, W.; Avezov, E.; Marsh, R. J.; Duchen, M. R.; Kaminski, C. F.; Bain, A. J. Investigating State Restriction in Fluorescent Protein FRET Using Time-Resolved Fluorescence and Anisotropy. *J. Phys. Chem. C* **2017**, *121* (3), 1507−1514.
(55) Blacker, T. S.; Mann, Z. F.; Gale, J. E.; Ziegler, M.; Bain, A. J.; Szabadkai, G.; Duchen, M. R. Separating NADH and NADPH Fluorescence in Live Cells and Tissues Using FLIM. *Nat. Commun.* **2014**, *5*, 3936.
(56) Zipfel, W. R.; Williams, R. M.; Christie, R.; Nikitin, A. Y.; Hyman, B. T.; Webb, W. W. Live Tissue Intrinsic Emission Microscopy Using Multiphoton-Excited Native Fluorescence and Second Harmonic Generation. *Proc. Natl. Acad. Sci. U. S. A.* **2003**, *100* (12), 7075−7080.
(57) Huang, S.; Heikal, A. A.; Webb, W. W. Two-Photon Fluorescence Spectroscopy and Microscopy of NAD(P)H and Flavoprotein. *Biophys. J.* **2002**, *82* (5), 2811−2825.
(58) Rover, L., Jr; Fernandes, J. C. B.; de Oliveira Neto, G.; Kubota, L. T.; Katekawa, E.; Serrano, S. H. P. Study of NADH Stability Using Ultraviolet−visible Spectrophotometric Analysis and Factorial Design. *Anal. Biochem.* **1998**, *260* (1), 50−55.
(59) de Wergifosse, M.; Elles, C. G.; Krylov, A. I. Two-Photon Absorption Spectroscopy of Stilbene and Phenanthrene: Excited-State Analysis and Comparison with Ethylene and Toluene. *J. Chem. Phys.* **2017**, *146* (17), 174102.
(60) Ramalingam, S.; Periandy, S.; Govindarajan, M.; Mohan, S. FT-IR and FT-Raman Vibrational Spectra and Molecular Structure Investigation of Nicotinamide: A Combined Experimental and Theoretical Study. *Spectrochim. Acta, Part A* **2010**, *75* (5), 1552−1558.
(61) Vasyutinskii, O. S.; Smolin, A. G.; Oswald, C.; Gericke, K. H. Polarized Fluorescence in NADH under Two-Photon Excitation with Femtosecond Laser Pulses. *Opt. Spectrosc.* **2017**, *122* (4), 602−606.
(62) Kasha, M. Characterization of Electronic Transitions in Complex Molecules. *Discuss. Faraday Soc.* **1950**, *9*, 14.
(63) Callis, P. R. On the Theory of Two-Photon Induced Fluorescence Anisotropy with Application to Indoles. *J. Chem. Phys.* **1993**, *99* (1), 27−37.
(64) Albinsson, B.; Norden, B. Excited-State Properties of the Indole Chromophore: Electronic Transition Moment Directions from Linear Dichroism Measurements: Effect of Methyl and Methoxy Substituents. *J. Phys. Chem.* **1992**, *96* (15), 6204−6212.
(65) Sobolewski, A. L.; Domcke, W. Ab Initio Investigations on the Photophysics of Indole. *Chem. Phys. Lett.* **1999**, *315*, 293−298.
(66) Kumar, M.; Jaiswal, S.; Singh, R.; Srivastav, G.; Singh, P.; Yadav, T. N.; Yadav, R. A. Ab Initio Studies of Molecular Structures, Conformers and Vibrational Spectra of Heterocyclic Organics: I. Nicotinamide and Its N-Oxide. *Spectrochim. Acta, Part A* **2010**, *75* (1), 281−292.
(67) Wu, Y. D.; Houk, K. N. Theoretical Study of Conformational Features of NAD+ and NADH Analogs: Protonated Nicotinamide and 1,4-Dihydronicotinamide. *J. Org. Chem.* **1993**, *58* (8), 2043−2045.
(68) Nakabayashi, T.; Islam, M. S.; Li, L.; Yasuda, M.; Ohta, N. Studies on External Electric Field Effects on Absorption and Fluorescence Spectra of NADH. *Chem. Phys. Lett.* **2014**, *595*, 25−30.
(69) Nelson, P.; Radosavljević, M.; Bromberg, S. *Biological Physics: Energy, Information, Life*; W. H. Freeman and Company: 2007.
(70) Wu, Y. D.; Houk, K. N. Theoretical Evaluation of Conformational Preferences of NAD+ and NADH: An Approach to Understanding the Stereospecificity of NAD+/NADH-Dependent Dehydrogenases. *J. Am. Chem. Soc.* **1991**, *113* (7), 2353−2358.
(71) Drobizhev, M.; Makarov, N. S.; Tillo, S. E.; Hughes, T. E.; Rebane, A. Two-Photon Absorption Properties of Fluorescent Proteins. *Nat. Methods* **2011**, *8* (5), 393−399.
(72) Drobizhev, M.; Tillo, S.; Makarov, N. S.; Hughes, T. E.; Rebane, A. Absolute Two-Photon Absorption Spectra and Two-Photon Brightness of Orange and Red Fluorescent Proteins. *J. Phys. Chem. B* **2009**, *113* (4), 855−859.
(73) Masters, T. A.; Marsh, R. J.; Armoogum, D. A.; Nicolaou, N.; Larijani, B. B.; Bain, A. J. Restricted State Selection in Fluorescent Protein Forster Resonance Energy Transfer. *J. Am. Chem. Soc.* **2013**, *135* (21), 7883−7890.

DOI: 10.1021/acs.jpcb.9b01236
J. Phys. Chem. B 2019, 123, 4705−4717